energies

Article

A Novel Data-Driven Estimation Method for State-of-Charge Estimation of Li-Ion Batteries

Suwei Zhai [1], Wenyun Li [2], Cheng Wang [3] and Yundi Chu [3,*]

[1] Electric Power Research Institute of China Southern Power Grid Yunnan Power Grid Co., Ltd., Kunming 650217, China; suwei_zhai@163.com
[2] Yunnan Power Dispatching Control Center of China Southern Power Grid, Kunming 650011, China; lwy6505@sina.com
[3] College of IOT Engineering, Hohai University, Nanjing 210098, China; 1662510325@hhu.edu.cn
* Correspondence: 20191011@hhu.edu.cn

Abstract: With the increasing proportion of Li-ion batteries in energy structures, studies on the estimation of the state of charge (SOC) of Li-ion batteries, which can effectively ensure the safety and stability of Li-ion batteries, have gained much attention. In this paper, a new data-driven method named the probabilistic threshold compensation fuzzy neural network (PTCFNN) is proposed to estimate the SOC of Li-ion batteries. Compared with other traditional methods that need to build complex battery models, the PTCFNN only needs data learning to obtain nonlinear mapping relationships inside Li-ion batteries. In order to avoid the local optimal value problem of traditional BP neural networks and the fixed reasoning mechanism of traditional fuzzy neural networks, the PTCFNN combines the advantages of a probabilistic fuzzy neural network and a compensation fuzzy neural network so as to improve the learning convergence speed and optimize the fuzzy reasoning mechanism. Finally, in order to verify the estimation performance of the PTCFNN, a 18650-20R Li-ion battery was used to carry out the estimation test. The results show that the mean absolute error and mean square error are very small under the conditions of a low-current test and dynamic-current test, and the overall estimation error is less than 1%, which further indicates that this method has good estimation ability.

Keywords: Li-ion batteries; state of charge; fuzzy neural network; data-driven

Citation: Zhai, S.; Li, W.; Wang, C.; Chu, Y. A Novel Data-Driven Estimation Method for State-of-Charge Estimation of Li-Ion Batteries. *Energies* **2022**, *15*, 3115. https://doi.org/10.3390/en15093115

Academic Editor: Truong Quang Dinh

Received: 24 March 2022
Accepted: 20 April 2022
Published: 24 April 2022

1. Introduction

With the increasingly serious problems of environmental pollution and energy shortage, related researchers all over the world are paying more and more attention to sustainable development [1–3]. Therefore, the existing energy structure is bound to change, and the proportion of clean energy in the energy structure will become higher and higher. A Li-ion battery is a typical application of clean energy because of its high energy density, small size, and good stability [4,5]. Especially in recent years, Li-ion batteries have been widely used in electric vehicles, various consumer electronics, microgrids and other fields [6–8]. State of charge (SOC) represents the remaining power of the battery, which can be defined as the ratio between the remaining capacity of the battery and the maximum capacity of the battery, and the SOC is an important basis for the safety control of the battery. In order to improve the safety performance and prolong the service life of a Li-ion battery, it is very important to estimate the SOC accurately.

At present, scholars have proposed various methods for the SOC estimation of Li-ion batteries, which can be summarized into two categories: the battery physical model prediction estimation method and data-driven estimation method [9–13]. Common methods of the former include ampere-hour integration and open-circuit voltage (OCV) [9,10]. The ampere-hour integral method is simple to calculate, and it only needs to integrate the current in the charging and discharging process of the Li-ion battery over time, so as to calculate the battery capacity variable of the Li-ion battery. However, the cumulative error of this method increases with time, so periodic calibration is required. An OCV has a good estimation result, but it requires a long time to rest the battery pack, so it is not suitable for real-time SOC estimation. Common methods of the latter include Kalman filtering (KF) and neural network (NN) [11,12]. KF has good stability and adaptability, but its estimation accuracy is highly dependent on the accuracy of the battery model, and at the same time, the calculation is large. The several classical methods mentioned above have their own advantages, but there are also some shortcomings; the neural network method with a high data learning ability can make up for these shortcomings [13].

An NN has the characteristics of universal approximation and has been applied to SOC estimation, and there is no need to build an additional complex battery model [12–16]. As long as there are enough learning samples for an NN to learn, it can extract the mapping relationship between measurable physical quantity and the SOC through training, and further build the neural network model. In general, using an NN to estimate the SOC is a nonlinear mapping problem, and it is very necessary to choose an appropriate neural network structure. In [17], an improved BP neural network method was proposed and successfully applied to the SOC estimation of lithium batteries. The BP neural network is sensitive to weight change and can easily fall into local optimal solutions. A probabilistic fuzzy neural network (PFNN) can solve this problem well, and has an excellent performance in dealing with uncertain problems. At present, it is widely used in the field of pattern classification and nonlinear mapping [18,19]. For example, in [18], a PFNN was applied to lithium battery charging, which could improve the transient characteristics of voltage regulation when the load changed, and therefore made lithium battery charging safer and more efficient. Although the PFNN is an improvement of the common fuzzy neural network (FNN), it has an inherent defect like the common FNN, that is, the fuzzy reasoning mechanism is relatively fixed. In order to solve this problem, a compensatory fuzzy neural network (CFNN) provides an extra degree of freedom for the fuzzy neural network through the compensatory learning algorithm, thus optimizing the fuzzy reasoning mechanism [20]. Many studies show that by combining the advantages of different algorithms, the shortcomings of a single method can be mutually compensated, and a better performance method can be obtained [21–24]. Therefore, in order to better estimate the SOC of Li-ion batteries, a probabilistic threshold compensation fuzzy neural network (PTCFNN) is proposed in this paper. The PTCFNN combines the advantages of a PFNN and CFNN, and introduces a threshold design on this basis. The purpose of designing a threshold is to retain only the important probability information and ignore the secondary probability information, so as to reduce the interference of unimportant information. The characteristics of the PTCFNN can be summarized as follows:

(a) The PTCFNN inherits the universal approximation property of the neural network and can obtain nonlinear mapping relations through data learning.
(b) The PTCFNN inherits the advantages of a PFNN. By calculating and transmitting the input probability information, the ability of the PTCFNN to deal with uncertain disturbances is improved, and the problem of the local optimal solution of the BP neural network is avoided.
(c) The PTCFNN contains a threshold design, so that only important network information is retained and useless network information is eliminated.
(d) The PTCFNN adds a fuzzy compensation strategy. The fuzzy reasoning mechanism of the PTCFNN is optimized by introducing an extra degree of freedom.

The rest of this paper is arranged as follows: In Section 2, the overall strategy for the SOC estimation is introduced. In Section 3, the network structure of the PTCFNN is introduced in detail. In Section 4, the specific learning process and learning strategy of the SOC estimation based on the PTCFNN are introduced. In Section 5, simulation examples are designed to verify the effectiveness of the PTCFNN. In the last section, Section 6, a conclusion of the research in this paper is made.

2. Estimation Scheme of State of Charge

The SOC of Li-ion batteries refers to the remaining capacity of the battery, usually defined as (1) [5,13], and the SOC is a physical quantity that cannot be measured directly and only can be estimated by various measurable physical quantities (e.g., current, voltage, temperature, etc.) under the working state of Li-ion batteries. A number of model-based approaches have been proposed for this purpose, and a common RC equivalent circuit diagram of Li-ion batteries is shown in Figure 1, where V_0 represents terminal voltage, V_1 represents open circuit voltage, V_2 represents polarization voltage, R_1 represents equivalent resistance, R_2 represents diffusion resistance, C_2 represents capacitance, I represents loop current, and Δd represents total disturbance [9–11,14].

$$\mathrm{SOC} = \frac{Q_c}{Q_{\max}} \times 100\% \tag{1}$$

where Q_c is current capacity, and $Q_{\max}$ is maximum capacity.

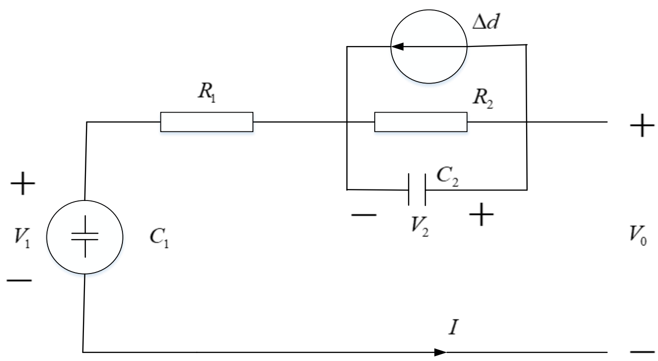

Figure 1. RC equivalent circuit diagram of Li-ion batteries.

However, it is not a simple problem to estimate the SOC through the equivalent model in Figure 1, because it is often necessary to set up several differential equations and consider the problem of unknown perturbation [25]. From the mathematical point of view, the SOC and these observable physical quantities are a multivariate nonlinear function relationship. In order to accurately obtain the nonlinear mapping relationship between these measurable physical quantities and the SOC, and avoid the establishment of additional complex physical and chemical models, this paper proposes a probabilistic threshold compensation fuzzy neural network, and the overall idea is shown in Figure 2. It should be noted that the PTCFNN is a data-driven method for the SOC estimation of lithium-ion batteries, and the nonlinear relationship inside the battery is learned through a large number of sample data.

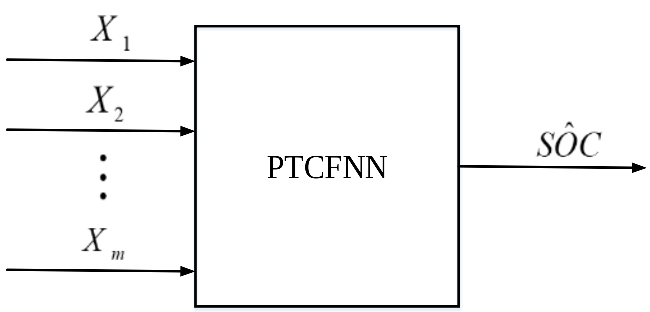

Figure 2. PTCFNN model.

As shown in Figure 2, the PTCFNN module represents the SOC estimator that has been learned, each measurable physical quantity is taken as the input of the PTCFNN, and the estimated value of the SOC is finally obtained through the nonlinear processing inside the PTCFNN. $X_k, (k = 1, 2, \cdots, m)$ represents the kth measurable physical quantity, $S\hat{O}C$ represents an estimate of the SOC obtained by the PTCFNN. The specific structure and data learning strategy of the PTCFNN will be introduced in the following two parts.

3. Probabilistic Threshold Compensation Fuzzy Neural Network (PTCFNN)

As the potential of neural networks to deal with nonlinear mapping has been developed, scholars have successfully applied neural networks to SOC estimation [12,13]. In this section, a probabilistic threshold compensation fuzzy neural network is introduced in detail. As shown in Figure 3, the PTCFNN has a total of eight layers of network structure, and each layer structure will be introduced in detail below.

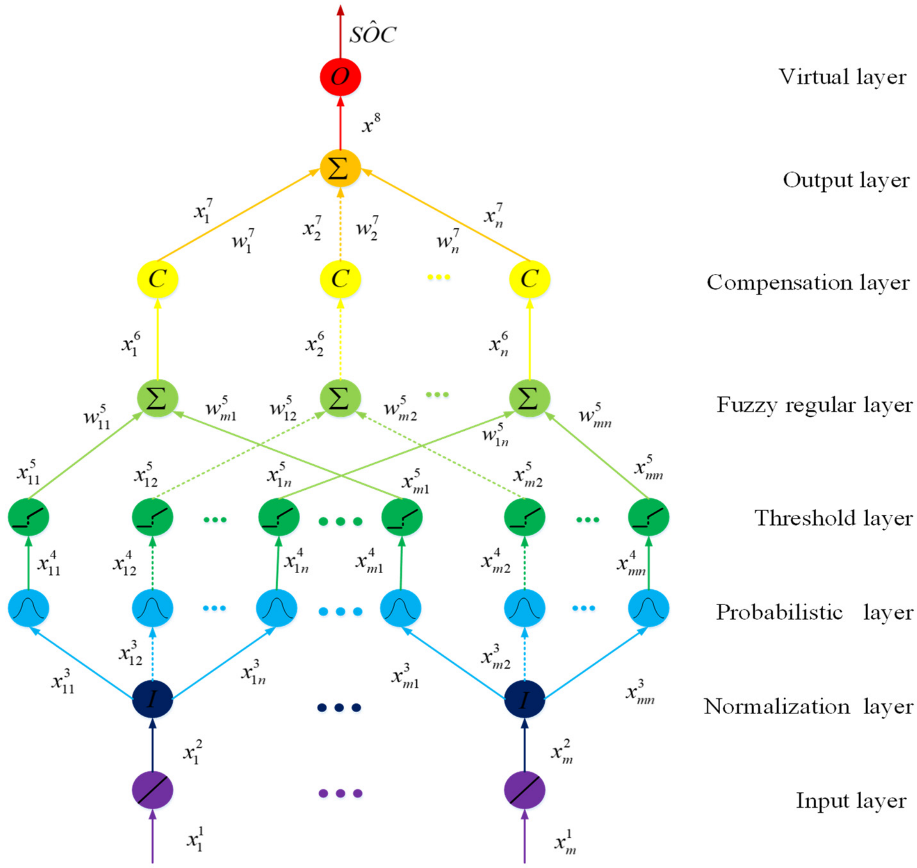

Figure 3. Structure of the PTCFNN.

1. Input layer.

This layer has m network nodes, which are used to transmit m measurable physical quantities. The specific input and output are defined as follows:

$$x_k^1 = X_k, k = 1, 2, \cdots, m \tag{2}$$

$$f_k^1 = x_k^1, k = 1, 2 \cdots, m \tag{3}$$

where x_k^1 is the kth input of this layer, and f_k^1 is the kth output of this layer.

2. Normalization layer.

In order to eliminate the adverse effects caused by singular sample data and improve the learning speed of the network, the normalization layer is introduced here, and its calculation method is as follows:

$$x_k^2 = f_k^1, k = 1, 2, \cdots, m \tag{4}$$

$$f_k^2 = \frac{x_k^1 - x_{k\min}^1}{x_{k\max}^1 - x_{k\min}^1}, k = 1, 2, \cdots, m \tag{5}$$

where x_k^2 is the kth input of this layer, f_k^2 is the k-th output of this layer, and $x_{k\max}^1$ and $x_{k\min}^1$ are the maximum and minimum values of the kth measurable physical quantity, respectively.

3. Probabilistic layer.

The probabilistic layer adopts a Gaussian radial basis function, and n classification nodes are designed artificially according to actual problems, and the input and output of each node are given by (6) and (7), respectively [16]. The purpose of introducing this layer is to make training easy and avoid the local minimum problem of a BP neural network.

$$x_{kj}^3 = f_k^2, k = 1, 2, \cdots, m; j = 1, 2, \cdots, n \tag{6}$$

$$f_{kj}^3 = \exp\left(\frac{(x_{kj}^3 - c_{kj}^3)^2}{2(b_{kj}^3)^2}\right), k = 1, 2, \cdots, m; j = 1, 2, \cdots, n \tag{7}$$

where c_{kj}^3 and b_{kj}^3 are, respectively, the center and width of the jth classification node corresponding to the kth normalized input. It should be pointed out that the input probability information calculated through (7) will be transmitted to the following layers.

4. Threshold layer.

Nodes in the threshold layer correspond to the nodes in the probability layer one by one. By setting the pass threshold, relatively important probability information can be retained, and the influence of secondary information can be reduced. The design idea is as follows:

$$x_{kj}^4 = \begin{cases} 0, f_{kj}^3 \le th \\ f_{kj}^3, f_{kj}^3 > th \end{cases}, k = 1, 2, \cdots, m; j = 1, 2, \cdots, n \tag{8}$$

$$f_{kj}^4 = x_{kj}^4, k = 1, 2, \cdots, m; j = 1, 2, \cdots, n \tag{9}$$

where th is the preset threshold.

5. Fuzzy regular layer.

In order to understand the influence of different inputs on the final output, a fuzzy rule is formulated as follows: the weighted sum of the outputs of a group of threshold layer is taken as the output of a node of fuzzy rule layer.

$$x_j^5 = \sum_{j=1}^{n} w_{kj}^4 f_{kj}^4, k = 1, 2, \cdots, m; j = 1, 2, \cdots, n \tag{10}$$

$$f_j^5 = x_j^5, j = 1, 2, \cdots, n \tag{11}$$

$$w_{kj}^4 = \exp(wi_{kj}^4), k = 1, 2, \cdots, m; j = 1, 2, \cdots, n \tag{12}$$

where w_{kj}^4 is the output weight of kj node with threshold layer label, and wi_{kj}^4 is the parameter of w_{kj}^4. It is important to note that the output weight w_{kj}^4 must be positive and the previous probability information has to be summed up, otherwise it will cause errors in the later compensation layer.

6. Compensation layer

The compensation layer introduces a group of free variables to the network, the fuzzy reasoning mechanism is optimized, and the network performance is better than that of common FNNs. The fuzzy compensation strategy is given by (14), and the design of each node is as follows:

$$x_j^6 = (x_j^5)^{1-c_j+c_j/m}, j = 1, 2, \cdots, n \tag{13}$$

$$c_j = \frac{1}{1+\exp(-ci_j)}, j = 1, 2, \cdots, n \tag{14}$$

$$f_j^6 = x_j^6, j = 1, 2, \cdots, n \tag{15}$$

where c_j is the free variable named compensation degree, and ci_j is the parameter of c_j, which is strictly limited from 0 to 1 [18].

7. Output layer.

The output layer has only one output node, which is the predictive output of the SOC estimation, which is obtained by the following formula:

$$x_j^7 = f_j^6, j = 1, 2, \cdots, n \tag{16}$$

$$f^7 = \sum_{j=1}^{n} w_j^7 x_j^7, j = 1, 2, \cdots, n \tag{17}$$

where w_j^7 is the output weight of the jth node in the compensation layer. It is worth noting that in order to accelerate the learning convergence speed of the PTCFNN, a normalized operation is applied to both the input and output of learning samples. Therefore, the SOC estimation results currently are normalized results, which need to be de-normalized at the next layer.

8. Virtual layer

The core structure of the PTCFNN is the first seven layers, and the existence significance of the virtual layer is only used for data processing to obtain the estimated value of the SOC. The calculation formula is given as follows:

$$x^8 = f^7(Q_{\max} - Q_{\min}) + Q_{\min} \tag{18}$$

$$S\hat{O}C = \frac{x^8}{Q_{\max}} \tag{19}$$

where $Q_{\min}$ is the minimum Li-ion battery capacity of learning samples.

The above is the introduction of the specific structure of the PTCFNN, and the strategy for the SOC estimation of the PTCFNN will be put forward in the next section.

4. SOC Estimation Based on the PTCFNN

In practical Li-ion battery applications, it is often difficult to establish an accurate battery model. The PTCFNN can overcome this shortcoming by building a nonlinear mapping model of measurable data characteristics and the SOC through a large amount of data learning, which is shown in Figure 2. The specific training process is shown in Figure 4 and can be summarized as follows:

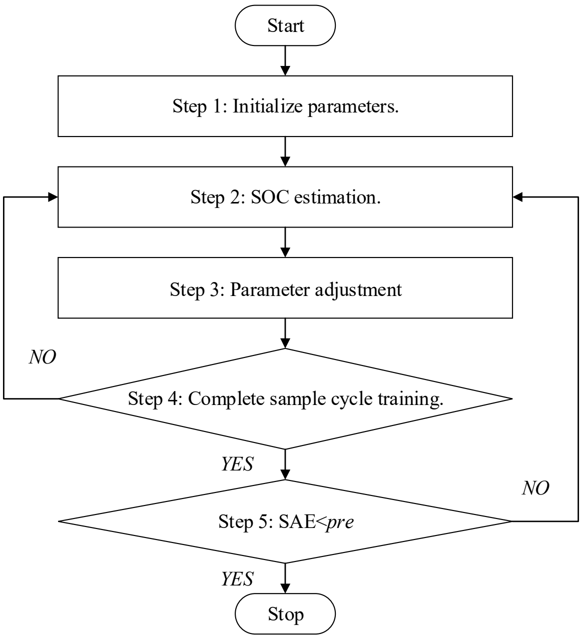

Figure 4. PTCFNN training process.

Step 1: Initialize necessary network parameters, including $x^1_{k\min}$, $x^1_{k\max}$, c^3_{kj}, b^3_{kj}, th, wi^4_{kj}, ci_j, $Q_{\max}$, $Q_{\min}$, m, n and *pre*.

$$pre = \sum_{i=1}^{N} |e_i| = \sum_{i=1}^{N} \left| SOC_i - S\hat{O}C_i \right| \tag{20}$$

where *pre* is the training indicator, and the sum of absolute errors (SAE) is adopted in this paper; N is the number of training samples; SOC_i is the reference output value of sample i; and $S\hat{O}C_i$ is the estimated output value of sample i.

Step 2: Perform the SOC estimation. The SOC of sample i will be estimated by the PTCFNN proposed in the previous section.

Step 3: Parameter adjustment. The loss function was defined as (21), and parameters were adjusted by the gradient descent method.

$$E = \frac{1}{2}\sum_{i=1}^{N} e_i^2 \tag{21}$$

It is worth noting here that only two groups of important parameters wi^4_{kj} and w^7_j are adjusted in this paper, and detailed adjustment formulas are given.

$$\begin{aligned} \Delta wi^4_{kj} &= -\eta_{wi^4} \tfrac{\partial E}{\partial wi^4_{kj}},\ k = 1, 2, \cdots, m;\ j = 1, 2, \cdots, n \\ &= \eta_{wi^4} e_i \tfrac{Q_{\max} - Q_{\min}}{Q_{\max}} w^7_j (1 - c_j + \tfrac{c_j}{m}) \tfrac{x^6_j}{x^5_j} f^4_{kj} w^4_{kj} \end{aligned} \tag{22}$$

$$\begin{aligned} \Delta w^7_j &= -\eta_{w^7} \tfrac{\partial E}{\partial w^7_j},\ j = 1, 2, \cdots, n \\ &= \eta_{w^7} e_i \tfrac{Q_{\max} - Q_{\min}}{Q_{\max}} x^7_j \end{aligned} \tag{23}$$

where $\eta_{wi^4} \in (0,1)$ and $\eta_{w^7} \in (0,1)$ are the learning rate, and e is the SOC estimation error of the ith sample

Considering the influence of last weight variation, momentum factor α is introduced, and the final weight is as follows:

$$wi_{kj}^4(k+1) = wi_{kj}^4(k) + \Delta wi_{kj}^4 + \alpha_{kj}^4(wi_{kj}^4(k) - wi_{kj}^4(k-1)) \tag{24}$$

$$w_j^7(k+1) = w_j^7(k) + \Delta w_j^7 + \alpha_j^7(w_j^7(k) - w_j^7(k-1)) \tag{25}$$

where α_{kj}^4 and α_j^7 are momentum factors; $wi_{kj}^4(k+1)$ is the next wi_{kj}^4, $wi_{kj}^4(k)$ is the current wi_{kj}^4, and $wi_{kj}^4(k-1)$ is the last wi_{kj}^4; $wi_j^7(k+1)$ is the next wi_j^7, $wi_j^7(k)$ is the current wi_j^7, and $wi_j^7(k-1)$ is the last wi_j^7.

Step 4: Judge whether a sample cycle training has been completed. If the sample number is N, go to the next step; otherwise, return to Step 2.

Step 5: Judge whether the current PTCFNN meets the set training indicator *pre*. If the current SAE is less than *pre*, the training ends; otherwise return to Step 2.

If the PTCFNN model can be learned through the above steps, it can be applied to the SOC estimation of Li-ion batteries. In the next part, the PTCFNN model learned will be applied to SOC estimation.

5. Simulation Results

In order to verify the feasibility of the PTCFNN in SOC estimations, the 18650-20R Li-ion batteries were selected as test samples, and their specific parameters are listed in Table 1. This section carries out two tests, namely a low-current test and dynamic-current test. It is worth noting that the learning data and test data came from the public battery data of the CALCE Battery Research Group [26], which were obtained when the temperature was constant. Therefore, the data at 0 °C were selected for testing in this paper. Detailed procedures for the two tests mentioned above are described below.

Table 1. Parameters of 18650-20R.

Battery (Parameters)	Specifications (Value)
Capacity rating	2000 mAh
Cell chemistry	LiNiMnCoO2/Graphite
Weight (with safety circuit removed)	45.0 g
Dimensions (mm)	18.33 ± 0.07 mm
Length	64.85 ± 0.15 mm
Nominal voltage	3.6 V

5.1. Low-Current Test

The low-current test consists of charging and discharging processes, and the mean absolute error (MAE) and root mean square error (RMSE) are introduced as reference indexes.

$$\mathrm{MAE} = \frac{1}{N}\sum_{i=1}^{N}|e_i| \tag{26}$$

$$\mathrm{RMSE} = \sqrt{\frac{1}{N}\sum_{i=1}^{N}{e_i}^2} \tag{27}$$

During the charging process, the fully discharged battery was charged at a stable current of 0.1 A, and the estimated SOC from 0 to 0.8 was observed and recorded. Figures 5 and 6, respectively, show the result of the SOC estimation and the relative error of the SOC estimation in the process of low-current charging. It can be seen that the overall estimation result is very good, and the relative error is stable within 1%. Figures 7 and 8, respectively, show the current and voltage in the charging process. It can be seen that the current is mostly stable at 0.1 A and the voltage shows a nonlinear growth trend. The MAE and RMSE of the test procedure were 0.0019 and 0.0027, respectively.

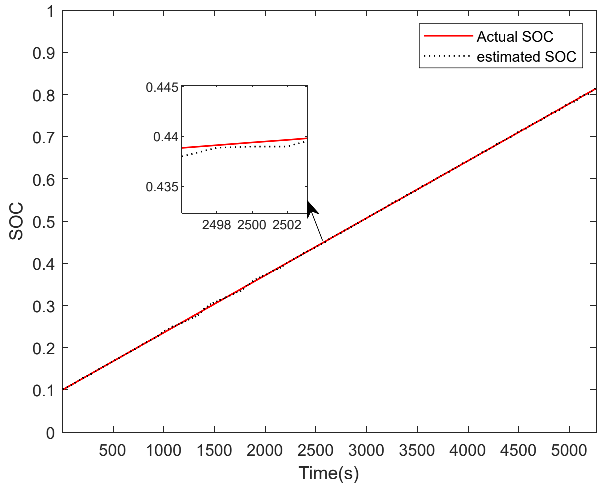

Figure 5. SOC estimation during low-current charging.

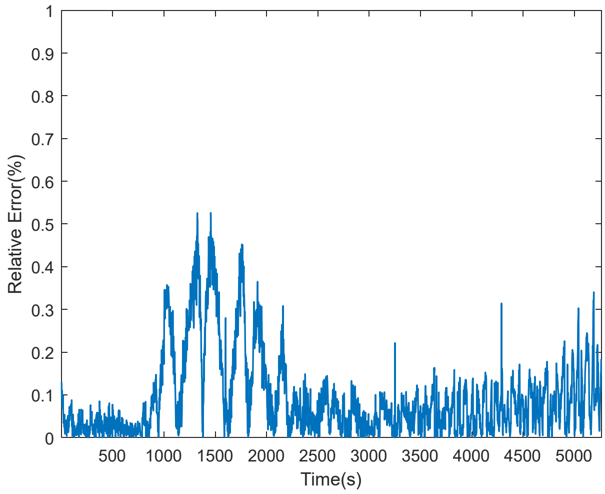

Figure 6. Relative error during low-current charging.

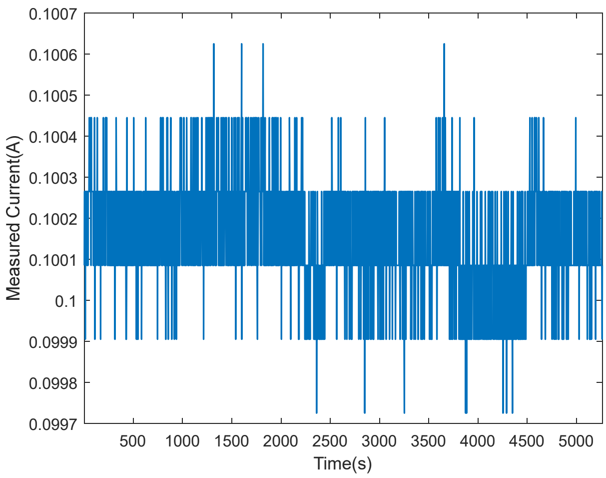

Figure 7. Measured current during low-current charging.

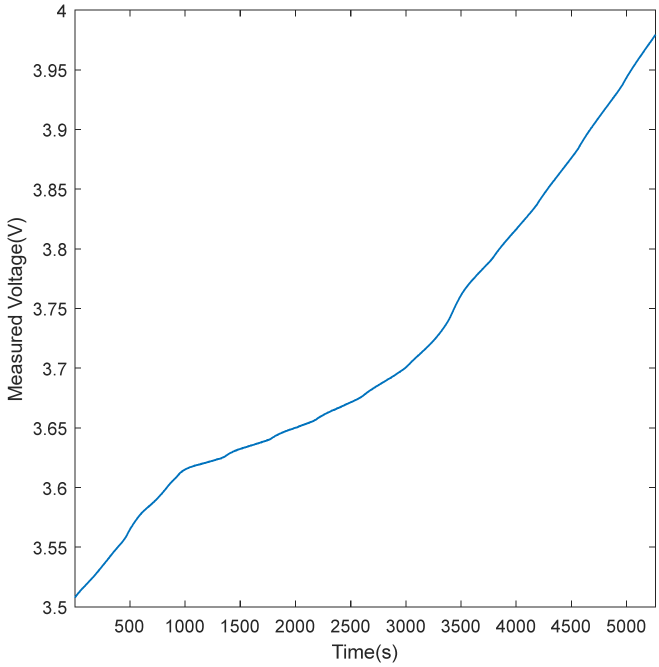

Figure 8. Measured voltage during low-current charging.

During the discharge process, the discharge test was also carried out with a steady current of 0.1 A, and the estimated results of the SOC from 0.8 to 0.1 were observed and recorded. Figures 9 and 10, respectively, show the result of the SOC estimation and the relative error of the SOC estimation in the process of low-current discharging. It can be seen that the overall estimation result is excellent, and the relative error is stable within 1%. Figures 11 and 12, respectively, show the current and voltage in the discharging process. It can be seen that the current is mostly stable at −0.1 A and the voltage shows a nonlinear decreasing trend. The MAE and RMSE of the test procedure were 0.0037and 0.0047, respectively.

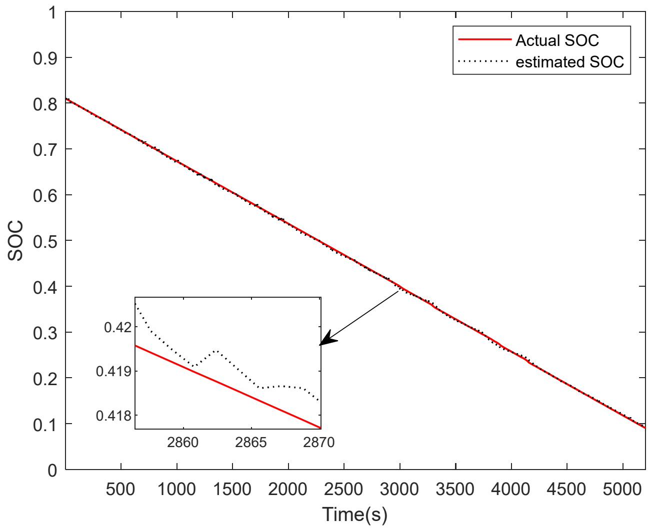

Figure 9. SOC estimation during low-current discharging.

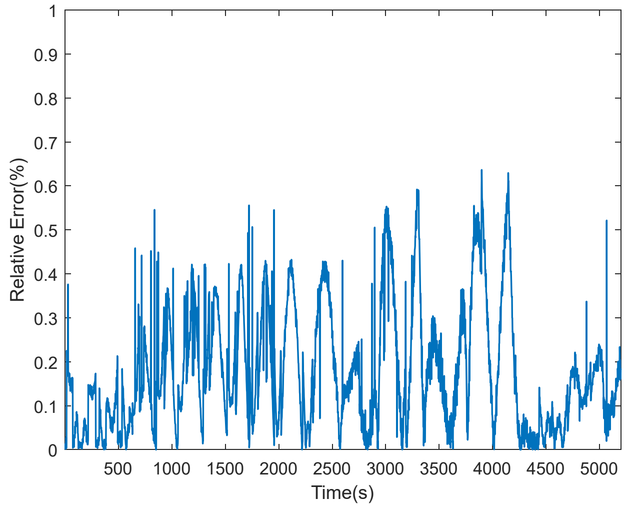

Figure 10. Relative error during low-current discharging.

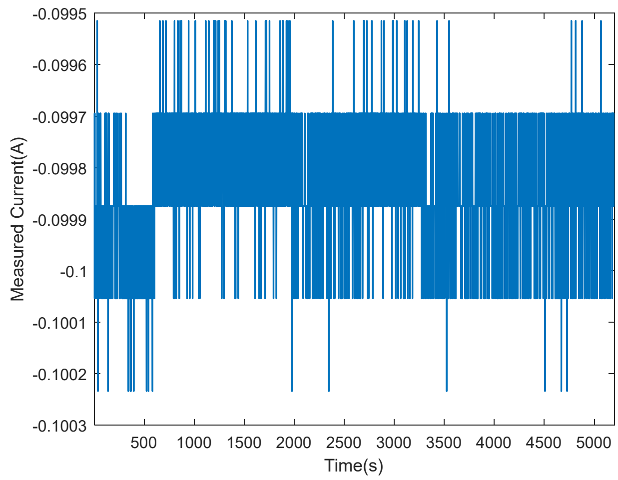

Figure 11. Measured current during low-current discharging.

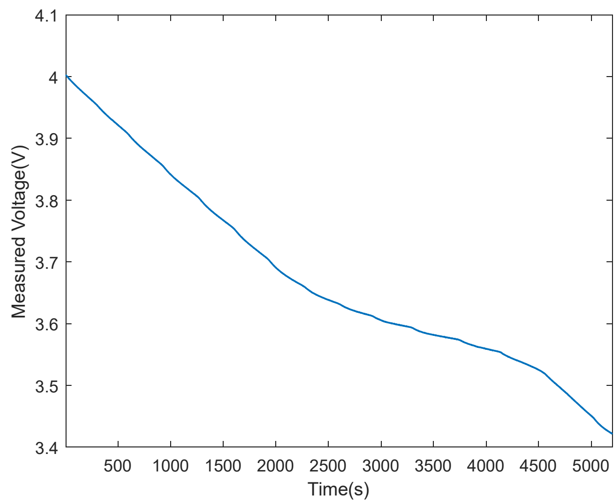

Figure 12. Measured voltage during low-current discharging.

The above test results show that the PTCFNN can perform the SOC estimation well in the process of stable low-current charge and discharge.

5.2. Dynamic-Current Test

Although the PTCFNN can perform SOC estimation well in the charging and discharging process of constant low current, the current is not constant in the actual battery charging and discharging process. For example, a new electric vehicle with a constant speed needs to provide a little more current when going uphill than when going downhill. To solve this problem, dynamic-current testing is performed in this section to observe and record the ability of the PTCFNN to estimate the SOC under dynamic current. The specific test process is to charge and discharge a lithium-ion battery with an SOC of 0.8 through dynamic current, and finally reduce its SOC to 0.1. Meanwhile, the SOC estimation result of a PFNN is compared with that of the PTCFNN.

Figure 13 shows the SOC estimation results of the FNN, PFNN and PTCFNN. It can be seen from the figure that these three methods can estimate the SOC of Li-ion batteries well. Figure 14 shows the relative estimation error of the FNN, PFNN and PTCFNN. It can be seen from the figure that the estimation error of the PTCFNN is less than 1%, while that of the PFNN is less than 3% and that of the PFNN is less than 10%. Therefore, by optimizing the inference mechanism, the estimation model using the proposed PTCFNN is ultimately more accurate. Figures 15 and 16 show the current and voltage in the test process, respectively. It can be seen that both the current and voltage are changing dynamically. The MAE and RMSE of the FNN, PFNN and PTCFNN are listed during dynamic-current testing in Table 2, in which the SOC estimation performance of the PTCFNN is better than that of the FNN and PFNN.

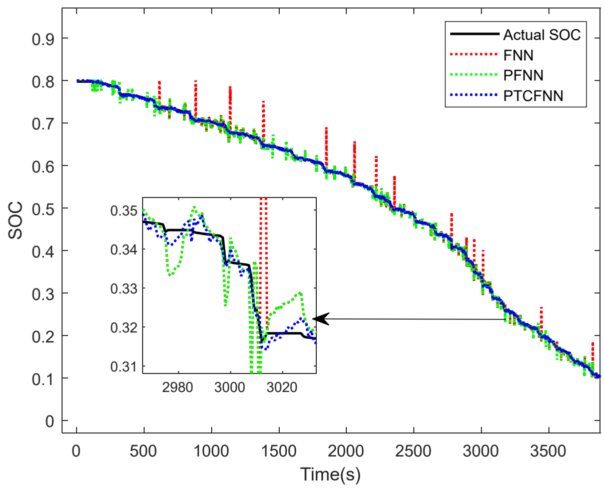

Figure 13. SOC estimation during dynamic current.

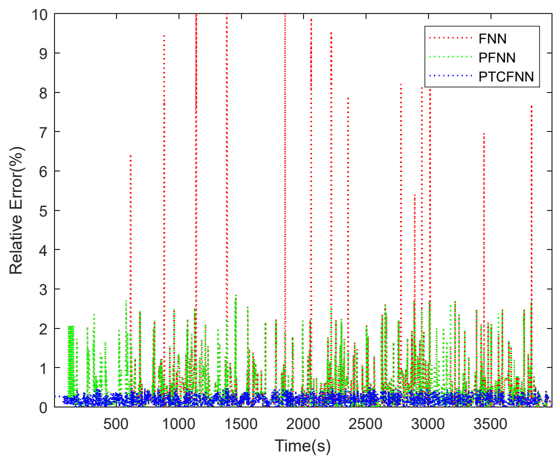

Figure 14. Relative error during dynamic current.

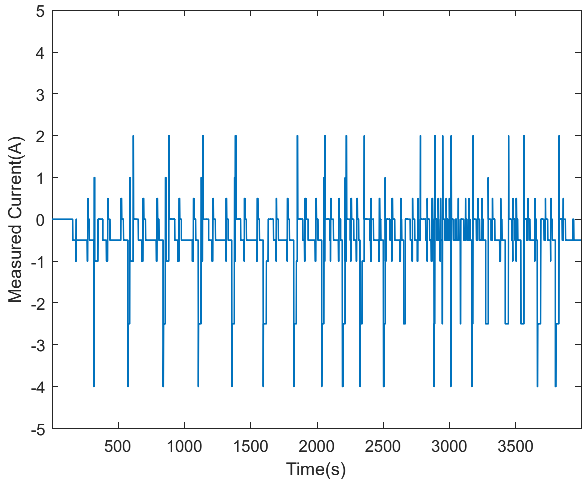

Figure 15. Measured current during dynamic current.

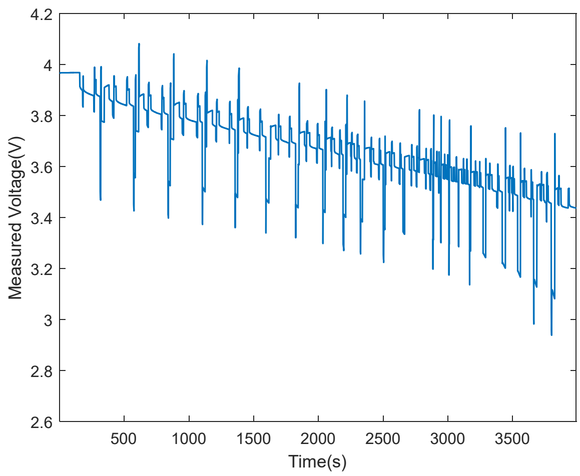

Figure 16. Measured voltage during dynamic current.

Table 2. MAE and RMSE.

Method	MAE	RMSE
FNN	0.0048	0.0098
PFNN	0.0041	0.0062
PTCFNN	0.0018	0.0022

5.3. Robustness Test

In order to verify the robustness of the PTCFNN, a 2% random relative error is added to the current measurement and voltage measurement, and the simulation results are shown in Figures 17–20. As can be seen from the simulation results, even when there are measurement errors, although a small part of the SOC estimation results have a deviation of more than 5%, the overall estimation error of the PTCFNN is less than 1%. The corresponding MAE and RMSE are 0.002 and 0.0032, respectively. Compared with the results without a measurement error, each indicator of the SOC estimation is not significantly damaged, so it can be considered that the proposed PTCFNN has good robustness.

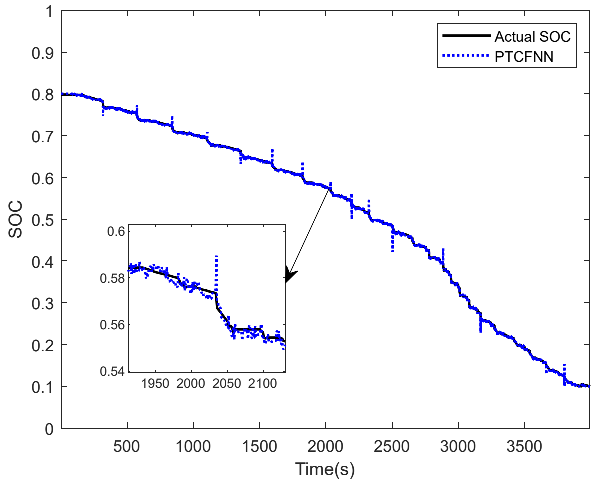

Figure 17. SOC estimation during dynamic current with disturbance.

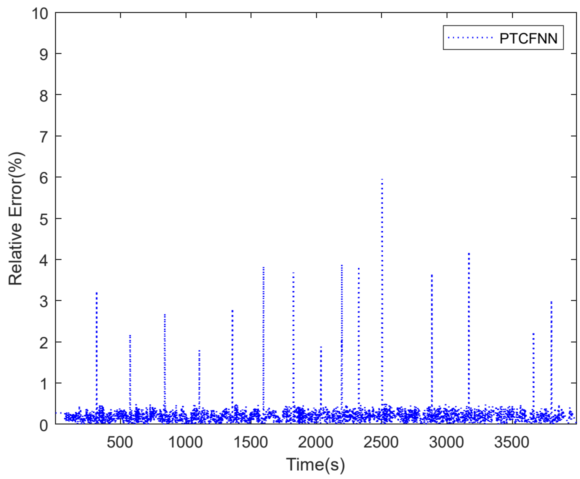

Figure 18. Relative error during dynamic current with disturbance.

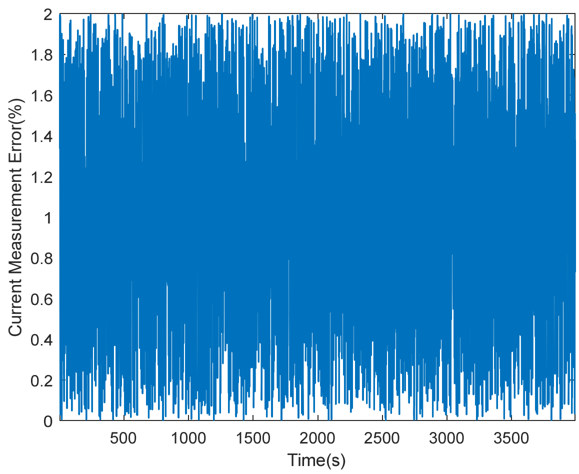

Figure 19. Current measurement error during dynamic current with disturbance.

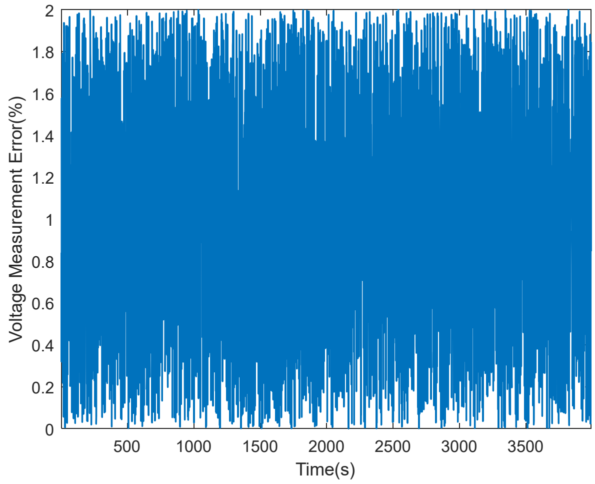

Figure 20. Voltage measurement error during dynamic current with disturbance.

Remark 1. *The initial parameter design of the PTCFNN is very important, and the initial parameters selected in this paper are as follows: The center* c^3_{kj} *of each node in the probability layer is n-section point from 0 to 1, the corresponding width* b^3_{kj} *is 1/n, and n = 100. The threshold is designed as th = 0.001,* ci_j *is designed as 0.5,* w^4_{kj} *and* w^7_j *are random numbers from 0 to 1, and other weights are set as 1. The parameters used for network adjustment are designed as* $\eta_{wi^4} = 0.01$, $\eta_{w^7} = 0.01$, $\alpha^4_{kj} = 0.001$ *and* $\alpha^7_j = 0.001$. *It is worth explaining that the above parameters are obtained through trial and error, and unreasonable parameter design will lead to learning failure. Generally speaking, the center of probability layer should cover the entire input space, and the corresponding width should not be more than half of the distance between adjacent centers. The degree of compensation is determined by the number of inputs and is designed to be* 1/2 *m.*

Remark 2. *The data-driven method is a popular research direction of nonlinear estimation at present* [12–16]. *The proposed PTCFNN is a newly data-driven SOC estimation method. The nonlinear relationship between input and output is extracted through network training, and then used for the SOC estimation of the Li-ion battery. Experimental results show that the PTCFNN has a good performance in the SOC estimation. However, the parameter selection of the PTCFNN relies heavily on empirical knowledge. In the future, self-organizing fuzzy neural network with full adjustment of the structure and parameters can be considered to optimize the PTCFNN for reducing its dependence on empirical knowledge.*

Remark 3. *When the SOC is more than 80%, the charge loss of the Li-ion battery is very high. Similarly, the Li-ion battery can over-discharge when the SOC is less than 10%. In order to ensure the efficient use of the Li-ion battery, the charge and discharge process of the Li-ion battery is often studied when the SOC is between 20% and 80%. Considering the above reason, research on SOC estimations in a certain range has become a mainstream direction* [27–31]. *Therefore, this paper studies the charge–discharge process of the SOC at 10% to 80%.*

6. Conclusions

In this paper, a probabilistic threshold compensation fuzzy neural network is proposed to estimate the state of charge of Li-ion batteries. The PTCFNN is essentially a data-driven method. On the one hand, by introducing a PFNN structure, the PTCFNN can avoid the local minimum problem of a BP neural network and accelerate the convergence speed. On the other hand, by introducing a CFNN structure, the PTCFNN makes up for the deficiency of a traditional fuzzy neural network, optimizes the fuzzy reasoning mechanism, and greatly improves the success rate of learning. Finally, the PTCFNN is applied to estimate the state of charge of a 18650-20R Li-ion battery. The test results show that the SOC estimation effect is very good in a low current and dynamic current. At present, the SOC estimation studied in this paper is carried out under a constant temperature. In the future, we will further study the SOC estimation under the scenario of temperature change and Li-ion battery aging. To handle different practical conditions (e.g., variable temperature, noise, and aging cycle), transfer learning can be a good choice, such that the mechanism combining PTCFNN with transfer learning will be exploited in future.

Author Contributions: Conceptualization, S.Z. and W.L.; methodology, S.Z. and W.L.; validation, S.Z., W.L. and C.W.; writing—original draft preparation, S.Z., W.L. and C.W.; writing—review and editing, S.Z. and W.L.; supervision, Y.C.; project administration, Y.C.; funding acquisition, Y.C. All authors have read and agreed to the published version of the manuscript.

Funding: This research was funded by the Science and Technology Project of China Southern Power Grid Yunnan Power Grid Co., Ltd., grant number YNKJXM20220048, China Postdoctoral Science Foundation, grant number. 2021MD703895, National Natural Science Foundation of China, grant number 62003132.

Institutional Review Board Statement: Not applicable.

Informed Consent Statement: Not applicable.

Data Availability Statement: Data sharing not applicable.

Conflicts of Interest: The authors declare no conflict of interest.

References

1. Cheng, Y.; Zhang, X.; Wang, X.; Li, J. Battery state of charge estimation based on composite multiscale wavelet transform. *Energies* **2022**, *15*, 2064. [CrossRef]
2. Guo, Y.; Lu, Z. A robust algorithm for state-of-charge estimation under model uncertainty and voltage sensor bias. *Energies* **2022**, *15*, 1537. [CrossRef]
3. Yuan, H.; Han, Y.; Zhou, Y.; Chen, Z.; Du, J.; Pei, H. State of charge dual estimation of a Li-ion battery based on variable forgetting factor recursive least square and multi-innovation unscented kalman filter algorithm. *Energies* **2022**, *15*, 1529. [CrossRef]
4. Jiang, Y.; Song, W.; Zhu, H.; Zhu, Y.; Du, Y.; Yin, H. Extended rauch-tung-striebel smoother for the state of charge estimation of Lithium-Ion batteries based on an enhanced circuit model. *Energies* **2022**, *15*, 963. [CrossRef]
5. Khalid, A.; Sarwat, A.I. Unified univariate-neural network models for Lithium-Ion battery state-of-charge forecasting using minimized akaike information criterion algorithm. *IEEE Access* **2021**, *9*, 39154–39170. [CrossRef]
6. Sun, Q.; Lv, H.; Wang, S.; Gao, S.; Wei, K. Optimized state of charge estimation of Lithium-Ion battery in SMES/battery hybrid energy storage system for electric vehicles. *IEEE Trans. Appl. Supercond.* **2021**, *31*, 1–6. [CrossRef]
7. Zhang, H.; Mo, Z.; Wang, J.; Miao, Q. Nonlinear-drifted fractional brownian motion with multiple hidden state variables for remaining useful life prediction of Lithium-Ion batteries. *IEEE Trans. Reliab.* **2019**, *69*, 768–780. [CrossRef]
8. Faisal, M.; Hannan, M.A.; Ker, P.J.; Lipu, M.S.H.; Uddin, M.N. Fuzzy-based charging-discharging controller for Lithium-Ion battery in microgrid applications. *IEEE Trans. Ind. Appl.* **2021**, *57*, 4187–4195. [CrossRef]
9. Liu, Z.; Li, Z.; Zhang, J. Alternate adaptive extended kalman filter and ampere-hour counting method to estimate the state of charge. In Proceedings of the IEEE International Power Electronics and Application Conference and Exposition (PEAC), Shenzhen, China, 4–7 November 2018; pp. 1–4.
10. Li, Y.; Guo, H.; Qi, F.; Guo, Z.; Li, M. Comparative study of the influence of open circuit voltage tests on state of charge online estimation for Lithium-Ion batteries. *IEEE Access* **2020**, *8*, 17535–17547. [CrossRef]
11. He, Z.; Yang, Z.; Cui, X.; Li, E. A method of state-of-charge estimation for EV power Lithium-Ion battery using a novel adaptive extended kalman filter. *IEEE Trans. Veh. Technol.* **2020**, *69*, 14618–14630. [CrossRef]
12. Hou, S.; Fei, J.; Chen, C.; Chu, Y. Finite-time adaptive fuzzy-neural-network control of active power filter. *IEEE Trans. Power Electron.* **2019**, *34*, 10298–10313. [CrossRef]
13. Hou, S.; Fei, J. A self-organizing global sliding mode control and its application to active power filter. *IEEE Trans. Power Electron.* **2020**, *35*, 7640–7652. [CrossRef]
14. Hou, S.; Chu, Y.; Fei, J. Robust intelligent control for a class of power-electronic converters using neuro-fuzzy learning mechanism. *IEEE Trans. Power Electron.* **2021**, *36*, 9441–9452. [CrossRef]
15. Hou, S.; Chu, Y.; Fei, J. Adaptive type-2 fuzzy neural network inherited terminal sliding mode control for power quality improvement. *IEEE Trans. Ind. Inform.* **2021**, *17*, 7564–7574. [CrossRef]
16. Hou, S.; Chu, Y.; Fei, J. Intelligent global sliding mode control using recurrent feature selection neural network for active power filter. *IEEE Trans. Ind. Electron.* **2021**, *68*, 7320–7329. [CrossRef]

17. Zhang, X.; Jin, Y.; Zhang, R.; Dong, H. Lithium battery SOC prediction based on mproved BP eural etwork algorithm. In Proceedings of the 3rd Asia Energy and Electrical Engineering Symposium (AEEES), Chengdu, China, 26–29 March 2021; pp. 882–886.
18. Lin, F.-J.; Huang, M.-S.; Yeh, P.-Y.; Tsai, H.-C.; Kuan, C.-H. DSP-based probabilistic fuzzy neural network control for Li-Ion battery charger. *IEEE Trans. Power Electron.* **2012**, *27*, 3782–3794. [CrossRef]
19. Capizzi, G.; Sciuto, G.L.; Napoli, C.; Połap, D.; Woźniak, M. Small lung nodules detection based on fuzzy-logic and probabilistic neural network with bioinspired reinforcement learning. *IEEE Trans. Fuzzy Syst.* **2019**, *28*, 1178–1189. [CrossRef]
20. Lin, F.-J.; Tan, K.-H.; Lai, Y.-K.; Luo, W.-C. Intelligent PV power system with unbalanced current compensation using CFNN-AMF. *IEEE Trans. Power Electron.* **2018**, *34*, 8588–8598. [CrossRef]
21. Merayo, N.; Juárez, D.; Aguado, J.C.; de Miguel, I.; Durán, R.J.; Fernández, P.; Lorenzo, R.M.; Abril, E.J. PID controller based on a self-adaptive neural network to ensure qos bandwidth requirements in passive optical networks. *J. Opt. Commun. Netw.* **2017**, *9*, 433–445. [CrossRef]
22. Chu, Y.; Fei, J.; Hou, S. Adaptive global sliding-mode control for dynamic systems using double hidden layer recurrent neural network structure. *IEEE Trans. Neural Netw. Learn. Syst.* **2019**, *31*, 1297–1309. [CrossRef]
23. Jin, Y.; Shan, C.; Wu, Y.; Xia, Y.; Zhang, Y.; Zeng, L. Fault diagnosis of hydraulic seal wear and internal leakage using wavelets and wavelet neural network. *IEEE Trans. Instrum. Meas.* **2018**, *68*, 1026–1034. [CrossRef]
24. Hou, S.; Wang, C.; Chu, Y.; Fei, J. Neural-observer-based terminal sliding mode control: Design and application. *IEEE Trans. Fuzzy Syst.* **2022**, 1–15. [CrossRef]
25. Feng, Y.; Xue, C.; Han, Q.; Han, F.; Du, J. Robust estimation for state-of-charge and state-of-health of lithium-ion batteries using integral-type terminal sliding-mode observers. *IEEE Trans. Ind. Electron.* **2020**, *67*, 4013–4023. [CrossRef]
26. CALCE Battery Research Group; University of Maryland: College Park, MD, USA. 2017. Available online: https://web.calce.umd.edu/batteries/data.htm (accessed on 25 July 2018).
27. Xiao, D.; Fang, G.; Liu, S.; Yuan, S.; Ahmed, R.; Habibi, S.; Emadi, A. Reduced-coupling coestimation of SOC and SOH for lithium-ion batteries based on convex optimization. *IEEE Trans. Power Electron.* **2020**, *35*, 12332–12346. [CrossRef]
28. Zheng, F.; Xing, Y.; Jiang, J.; Sun, B.; Kim, J.; Pecht, M. Influence of different open circuit voltage tests on state of charge online estimation for lithium-ion batteries. *Appl. Energy* **2016**, *183*, 513–525. [CrossRef]
29. Xing, Y.; He, W.; Pecht, M.; Tsuia, K.L. State of charge estimation of lithium-ion batteries using the open-circuit voltage at various ambient temperatures. *Appl. Energy* **2014**, *113*, 106–115. [CrossRef]
30. Oh, H.; Jeon, J.; Park, S. Effects of battery model on the accuracy of battery SOC estimation using extended kalman filter under practical vehicle conditions including parasitic current leakage and diffusion of voltage. *Int. J. Automot. Technol.* **2021**, *22*, 1337–1346. [CrossRef]
31. Zhou, S.; Chen, Z.; Huang, D.; Lin, T. A fault-tolerant SoC estimation method for series—parallel connected Li-Ion battery pack. *IEEE Trans. Power Electron.* **2021**, *36*, 13434–13448. [CrossRef]